**Advanced Steel Construction** – Vol. 18 No. 1 (2022) 495–505
**DOI:**10.18057/IJASC.2022.18.1.8


# NUMERICAL STUDY OF TWO NOVEL CONNECTIONS WITH SHORT END I OR H STUB IN STEEL STRUCTURES

Mehrdad Taheripour [1], Farzad Hatami [1, 2, *] and Reza Raoufi [1]

[1] *Department of Civil Engineering, Ahvaz Branch, Islamic Azad University, Ahvaz, Iran*
[2] *Department of Structures and Earthquake Research Center, Amirkabir University of Technology, Tehran, Iran*
** (Corresponding author: E-mail: hatami@aut.ac.ir)*

**ABSTRACT**

In this study, two novel steel connections are introduced by replacements in the conventional end-plate connection with an H-or I-shaped cross-section as a Short Stub Column (SSC). In the first connection, the SSC flange is bolted to the column flange, and the beam is welded to the stub flange. In the second connection, after welding the SSC flange to the column flange and welding the beam to an end-plate, the end-plate is bolted to the SSC flange. The flange and web of the stub are reinforced using horizontal stiffeners to transfer the beam moment. Stiffeners could be employed with various thicknesses and configurations such that the strength and ductility of the joint could be adjusted. In this study, the Finite Element Model (FEM) model of a conventional welded and bolted end-plate connection, subjected to cyclic loading, is primarily calibrated using experimental data from previous studies. After confirming the model's performance, the behavior of the two proposed connections, in comparison with it, has been studied. The hysteresis diagrams have been obtained for each case, followed by extracting the effective parameters and comparing them. The results show that the two Proposed Connections reduce the stress in the panel zone and increase the ductility compared to the previously confirmed end-plates. All the samples in this study satisfy the fundamental requirements for rigid beam-to-column connections, according to AISC.

**ARTICLE HISTOR**

Received: 17 December 2020
Revised: 16 June 2021
Accepted: 4 July 2021

**KEYWORDS**

Bolted end-plate connection;
Stub steel connections;
Panel zone;
Hysteresis diagrams;
PEEQ



## 1. Introduction

The seismic performance of steel frames is determined mainly by the connecting properties of the structures. The results of previous studies have shown that semi-rigid connections have outstanding properties, which make them proper substitutions for fully rigid connections. These properties are necessary for a smaller base shear, a better economy, and a better capability to absorb energy [1]. In addition to resisting shear, bending, and torsional forces to successfully transfer these internal forces from the beam to the column, connections must have sufficient capacity for deformation and provide the required ductility. Therefore, specific regulations have been formulated for connections under static and dynamic loading. Accordingly, extensive studies have been conducted, and several novel connections for connecting I-beams to columns have been proposed since the 1994 Northridge earthquake [2]. However, there is a need for more laws to be regulated for newly proposed connections [3]. Nevertheless, researchers are yet looking for a suitable beam-to-column joint [4]. Yielding is necessary for plastic energy to be absorbed. Brittle fracture of the connection prevents bending connections from exhibiting the non-elastic behavior required for resisting earthquake loads. Triaxial stresses have a substantial effect on ductility reduction and the appearance of brittle behavior. When steel is loaded simultaneously in two or three directions, it could not exhibit its inherent ductility; instead, it experiences brittle fracture without elongation [5]. Tremblay et al. [6,7] investigated steel structure performance during several earthquakes. Fractures caused by weak joints during the cyclic loading process demonstrated that, before the 1994 Northridge earthquake, design criteria did not practically result in the establishment of plastic hinges in the beam. After the Northridge earthquake, the primary goal was to move the plastic hinge inside the beam at a specified location from the column in the conventional connection. In these connections, placing the plastic hinge establishment farther from the column reduces strain concentration in the weld, hence, prevents the distribution of cracks in the weld and brittle fracture in the connection [8]. Various methods have been proposed for transferring the location of the plastic hinge formations. These methods are generally divided into two categories. In the first category, the connections are designed so that components' addition to the connection improves the beam strength. Thus, it transfers the plastic hinge inside the beam and prevents the rotation of the connection components concerning each other (beam concerning column). In the second group, a specific pre-determined region is weakened by reducing the section in areas of the flanges; therefore, the plastic hinge is transferred inside the beam. Various Reduced Beam Section (RBS) connections belong to this group [9].

Moreover, several attempts have been made to transfer the connections at a specific distance from the column using a stub. Behrooz et al. [10] used a short beam stub for steel connection. Shen [11] investigated two types of experimental replaceable connections using the reduced beam cross-section theory. This connection is a combination of end-plate and stub. Moreover, a replaceable link with a smaller cross-sectional area (than the beam) was used to generate the plastic hinge in the link. Li [12] studied a particular type of reverse channel connection in which the UNP webs are welded to box columns, and the UNP flanges are connected to the beams. Yılmaz et al. [13] used a stub in the form of a short beam along the weak axis of the column. Moghadam et al. [1] used two parallel connection plates welded vertically to the column and connect them to the beam using a flash end-plate. Gaoxing et al. [14] presented a replaceable energy dissipation system for connections of beams to concrete columns using a steel stub consisting of a short link and an H-shaped steel section with an open web. Han et al. [15] utilized a stub made of a shear hinge and a couple of buckling-restrained plates to present a beam-to-column connection for controlling seismic damages.

Qiang et al. [16] proposed a semi-rigid joint along the weak axis of the column, where the beam was attached to the web column by a combination of the transverse, vertical stiffeners, and flash end-plate connection, which formed a stub. Jiang et al. [17] proposed a novel connection in which vertical pair through-plates pass within box-column, and these plates bolted to web beam. Zhang et al. [18], using a stub attached to the beam and steel strands, suggested a premade self-centering steel structure with a novel floor system that includes movable minor beams for frame development. Liu et al. [19] proposed connection consists of two identical half-cylindrical parts connected to the column on one side with an end-plate and on the other side with a fin-plate to the beam. By rotating the fin plate relative to the end-plate, the half-cylindrical parts provide axial ductility.

In conventional rigid joints, the bending moment is transmitted from the beam to the column as a combination of compressive and tensile forces. Consequently, the two concentrated forces are applied to the column at the connection location, leading to higher stress in the panel zone. Moreover, an increase in the strength and hardness of the connection reduces its ductility. Additionally, a strong connection results in transferring all of the forces and moments, especially to the panel zone of the column, making it damageable. Therefore, using the extended surface section in the connection increases the contact surface between the connection, the column flange, and the force's distribution applied to the column. In addition to improved ductility, this reduces the stress involved in the panel zone. Thus, the idea of a flexible connection and reducing the damage to the column was proposed. This study attempted to combine the stub and end-plate connections to introduce two novel connections with a straightforward design and various behavior. The two Proposed Connections consist of an H- or I-shaped cross-section placed between the beam and column along its main axis. This connection prevents damage to other structural components by changing to plastic behavior. Upon using a stub, the plastic hinge moves far from the column. Moreover, the stress

in the panel zone is reduced by increasing the column's force transfer surface. Rolled profiles in the connection (where redundant parts could also be used) with a stiffening plate facilitate flexibility in the connection behavior, and the ductility and rigidity of the connection could be easily modified if required.

## 2. Two proposed connections

### *2.1. Proposed connection model (I)*

The proposed connection Model (I), as illustrated in Fig. 1, is located between the beam and column along its main axis as a Short Stub Column (SSC) using an H- or I-shaped cross-section. This stub is placed so that one of its flanges bolted to the column, and the other welded to the beam. Therefore, the web and flanges are reinforced with stiffeners to compensate for the stub inertia moment lack related to the beam. These stiffeners are directed along the beam flanges so that eccentricity does not generate moment and pry action in the stub flanges. If the thickness of the stiffeners is greater than the thickness of the beam flanges, the SSC connection acts as fully rigid, and a plastic hinge is an establishment in the beam. Furthermore, if the thickness of stiffeners is less than that of the beam flanges, the stub acts as a damper, and a plastic hinge gets formed in it. The height of the stub is more than that of the beam in the two Proposed connections. The connection quality is high due to the performance of all the weldments before assembling the structure. The width of the stub flanges must be more than the width of the beam flanges and at most equal to the flange width of the column. Complete Joint Penetration (CJP) groove welds are used to connect the web and flanges of the beam to the stub flange and the continuity plates to the stub. In this connection, a panel zone similar to that in the column is created in the stub web. This reduces stress in the panel zone of the column. The pry action due to the bolts causes bending between the two bolts, wherever the stub flange is bolted to the column. The stub's presence of stiffener plates causes the redistribution of stress among the flanges, the stub's web, and all the connection parts in resisting the exerted forces. Moreover, different thicknesses can be used for the stiffeners. The extended parts outside the beam height in the stub act as a haunch connection and transfer a considerable force to the outside bolts. The significant displacement at the beam's end causes substantial, large deformation and plastic strain at the extended part outside the beam height on the one hand and buckling at the opposite extended part on the other hand. This leads to a more considerable contribution of the stiffener plates to the force transfer and creating the stub flange's pry action. The increase in the displacement leads to the fracture of extended parts in the stub web, and tensile and compressive forces are transferred using stiffener plates. Finally, with an increase of pry action due to the bolts, the stub web suffers a fracture between the bolts, and the connection fails.

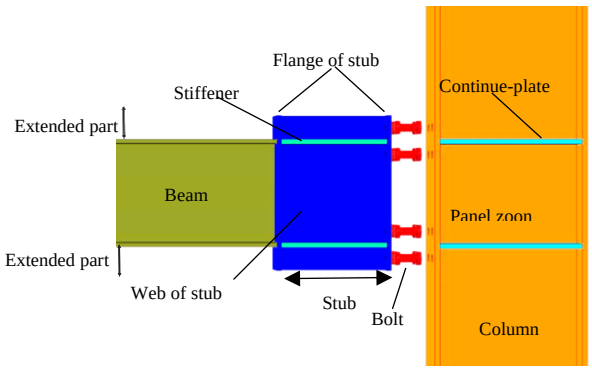


**Fig. 1** configuration setup of proposed Connection model(I)

### *2.2. Proposed connection model (II)*

In the proposed connection Model (II), as illustrated in Fig.2, one of the stub flanges is welded to the flange of the column, and the beam with the end-plate welded is bolted to the other stub flange. The end-plate width is equal to the stub flange width. Similar to model (I), the stub's web and flange are reinforced using stiffeners, and all the welds are applied at the factory. Moreover, the presence of a bolt layer in the connection results in better ductility. This connection is a suitable alternative to the tree connection. Like model (I), a panel zone formed in the stub web resembles this connection in the column. Due to the bending of the beam, the tensile and compressive forces are passed to the end-plate, then transmitted from the end-plate to the stub flange using bolts. Then, pry action causes the bending of the stub flange between the bolt rows. The stiffeners and stub web presence create a cross-shaped stiffener, which reduces the pry action in the bolts and redistributes the stress among the stub section elements. Therefore, the stress is transferred to the beam on a greater surface (equal to the surface area of the stub flange), finally reducing stress in the column's panel zone.

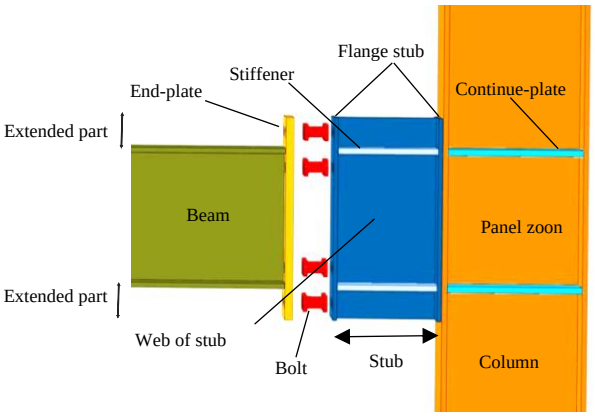


**Fig. 2** configuration setup of proposed Connection model(II):

## 3. Numerical modeling

The experiments for parameters study on the behavior of the connection are time-consuming and costly. With the technological advancement in recent years and the FEM development, computer simulation could be a proper alternative to experimental methods. Accordingly, finite element software with the nonlinear analysis capability was employed in this research.

### *3.1. Part modeling*

All sections are modeled as separate mechanical parts. The part type is 3D and deformable. The section drawing type, which determines the element base, is set to solid. The critical point in the initial drawing of the section is modeling the bolt since it acts as the interface between the stub with other parts of the connection and is in contact with all. Every bolt consists of a head, body, and a nut. The stub flange is in contact with the head, the nut is in contact with the column flange or end-plate, and the body of the bolt is in contact with the hole. Since modeling the bolt parts increases the number of modeled parts individually and increases the analysis time, all three parts are modeled as one part. The next point is modeling the weld. In the first few models, the weld was modeled with a triangular solid section. However, since it did not affect the results but increased the analysis time exponentially, modeling the weld was avoided in the final models, and the constraining property was used.

### *3.2. Material properties*

The material properties are introduced using a stress-strain curve. This curve is defined in two separate sections: elastic and plastic. In the elastic state, the material properties are isotropic, and the only inputs are the Poisson's ratio and modulus of elasticity. The data for plastic stress and strain are obtained in several points by utilizing the stress-strain curve. It must be noted that the introduced strain must not be the sum of elastic and plastic strain, and only the plastic strain must be introduced. Accordingly, the first input plastic strain corresponds to the yield stress and is equal to zero. The plastic properties of materials can change with the strain rate. Flow plasticity theory was used as the nonlinear behavior in this research. According to this theory, the response of materials after the initial yield leads to the redistribution of stress and forms a new yield level. With an increase in loading, this process continues up to the whole section's yielding and fracture. The reason for the resistance of steel after yielding is the hardening phenomenon. Accordingly, the stress-strain curve has been idealized using three lines to introduce the hardening behavior. The Von Mises yield criterion is used to evaluate whether a material has become plastic. Kinematic and isotropic hardening has been combined for consideration in the nonlinear behavior of materials. Two types of stress-strain curves have been used in this model. The first curve corresponds to common steels with which structural components are built. They are considered low-carbon steels and used in all parts of the beam, column, end-plate, and stiffeners (Fig. 3.a). The second curve (Fig. 3.b) was idealized for high-strength steels (bolts) [20].

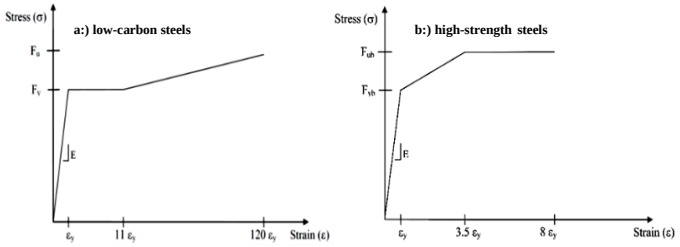


**Fig. 3** Stress-strain curves

### 3.3. Step analysis

The analysis type is determined by the model conditions, loading, contacts, and supports. Loading on the experimental model is performed at a low rate. Therefore, the static general analysis type is appropriate. This type of analysis could solve and simulate lateral buckling, rotational loading, and nonlinear behavior of materials. Two analysis steps have been considered in this model. In the first step, the bolt pretension force is applied. The end of the beam was subjected to cyclic loading in the second step. The effect of nonlinear geometry was taken into account in the second step to compute the large displacements more accurately.

### 3.4. Contact modeling

One of the complicated steps in simulating bolted connections is introducing the contact elements. Both models have 62 interactions. A contact element includes two critical parameters. The normal contact behavior parameter causes hard contact and prevents the surfaces from penetrating each other. The tangential behavior parameter defines the friction coefficient, which is 0.3. Overall, there will be three contact groups in this model. The first group corresponds between the stub flange with the column flange and the end-plate. The second group is the head's contact and the bolts' nut with the plates and the column flange. The third group is the contact between the bolt bodies and the holes. All the contacts are defined as surface-to-surface. The small sliding mode is defined as the contact between the plates, the bolts, and holes. This mode makes it possible for the bolts and plates to slide along each other. The finite sliding mode is used to contact the nut and the bolt head to prevent sliding and looseness. The tolerance for the adjustment zone factor is taken to be 0.05 for all three groups. The weld is not modeled in this research; thus, we must define the corresponding components of the connection. We use the constraint property for this purpose. The beam's connections with the end-plate and the column web's continuity plates are defined using this property. This property indicates the constraints applied to the Degrees of Freedom (DOFs) in the analysis because of a part's motion in the model. Furthermore, the tie constraint is used. This constraint makes it possible to combine two regions with different meshes. In this mode, the DOFs of the slave surface nodes are constrained by the DOFs of the master surface nodes. In this mode, the node-to-node constraint will be used, and only the beam borderlines are selected so that the force transfer is similar to that in weld lines.

### 3.5. Loading and boundary conditions

Displacement control is used to apply load to the end of the beam, and the displacement perpendicular to the load direction is limited to prevent lateral torsional buckling. The pretension force is applied in the first loading step. The bolt pretension force is applied to a virtual plane in the bolt body. The force must create stress equal to 70% of the bolt's maximum capacity [21]. This force is obtained 613 kN using trial and error in this model. In the second step, loading is applied using displacement control. The loading history is suggested by AISC 341-10 [22] and the SAC / BD-97/02 [23]. This protocol is based on the relative rotation of the beam end. The sample was loaded statically using displacement control. Besides, the beam end displacement is obtained by multiplying the drift angle by the beam length. The moment exerted on the connection is equal to the resulting force, multiplied by the distance between the beam end and the column center.

### 3.6. Meshes and element types

The last step in modeling is meshing and assigning elements to parts. The number of meshes and elements has a direct impact on the accuracy of the responses. Since meshing is carried out in three-dimensional space, and regular meshing has the highest quality, one must partition the parts into simpler components. Regular meshing partitions the part using hexahedral elements and provides 8-node and 20-node elements. The higher the seed density, the finer the created meshes, the more realistic the deformations, and the longer the analysis time. Therefore, seed density must be optimized. To this end, fine meshing will be selected only around the connection core. Thus, partitioning is implemented in the beam and the column at a distance equivalent to the beam height from the connection center. The seeding density was considered 10 in this part (the connection has been modeled on a mill metric scale) and 20 in other parts. Moreover, the seed density of the bolt is equivalent to four. Two element types have been used in this model: The C3D8R element, which is linear with eight nodes, and the C3D20R element, which is quadratic with 20 nodes. The beam and the bolt have been modeled using 20-node elements, and the other members have been modeled using 8-node elements. Both element types have plastic, hardening, and extensive deformation capabilities with 3 DOFs in each node. They could exhibit nonlinear behavior with reduced Gaussian integration points.

### 3.7. Verification

The crucial point in a simulation is examining and verifying the results. Thus, the SSC connection was compared to a pre-verified AISC connection to evaluate seismic behavior. The connections in this study are combinations of bolt and weld and are based on end-plate theory. Therefore, the model selected for verification was a beam-to-column connection using an extended unstiffened end-plate connecting to the column flange with four bolts on both sides of each beam flange. This connection is unidirectional and subjected to cyclic loading, in which the moment-rotation curve was investigated. The finite element model was validated using Sumner's [20] experimental model. This experiment involves a beam with a length of $432\,mm$ (from the beam tip to the column center) with a cross-section of $w24 \times 68$. It is connected in cantilever configuration to a column with a length of $556\,mm$ and a $w14 \times 120$ section using an extended end-plate with a thickness of $39\,mm$ and bolts with diameters of $38\,mm$. The structure is assembled horizontally, and a hydraulic jack is used to apply force to the beam's end (Fig. 4). The loading location has been reinforced using stiffeners to prevent the beam flange from crushing. The end of the beam has been restrained using the side support to prevent lateral torsional buckling. The beam and the column properties presented in Table 1, and those of the end-plate displayed in Fig. 5 and Table 2.

**Table 1**
Dimensions of the Sumner sample's beam and column

| | Length | Section depth | Width flange | Flange thickness | Web thickness |
|---|---|---|---|---|---|
| Beam(mm) | 4128 | 606 | 233 | 15 | 11 |
| Column(mm) | 5553 | 368 | 375 | 24 | 15 |

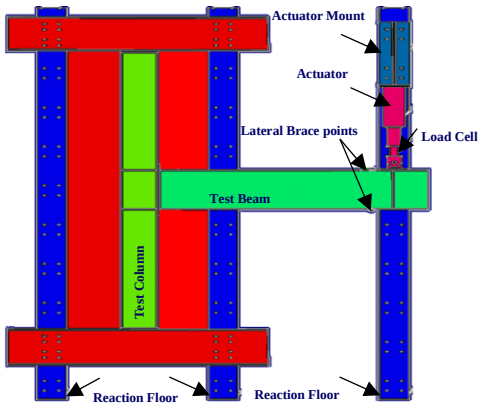


**Fig. 4** Geometric typical test setup of the Sumner sample [20]

**Table 2**
Data of extended end-plate used in the Sumner specimen [20]

| Parameter | tp | bp | Lpl | g | pf | pt | g | pf | pt |
|---|---|---|---|---|---|---|---|---|---|
| Built-Up(mm) | 39 | 254 | 857 | 152 | 43.4 | 71.4 | 151 | 53 | 63 |

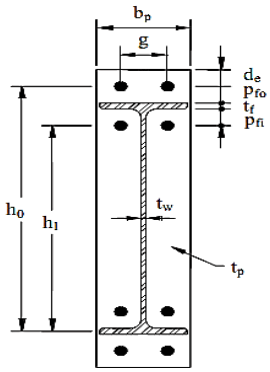


**Fig. 5** Details of extended end-plate

The modeling results in this study were validated by comparison with the results of the described sample. The rotation hysteresis curve against the bending moment was plotted (Fig. 6). In this curve, the rotation is obtained by dividing the beam's displacement by the distance between the beam's free end and the center of the column (sum of the beam length, end-plate thickness, and half of the column height). The moment is equivalent to the shear force product at the end of the beam and its distance from the column center. The FEM results are, as evident, compatible with the experimental results. The experimental model differs from the FEM model for a variety of reasons. One reason is that the stress-strain curve introduced to the software does not accurately represent the material's behavior. This is especially true for the bolts, which are high-strength and do not have a specific point of yield or fracture. The contact element created can also introduce errors since this element has a complex behavior, and the friction coefficient is not equivalent to the actual value. The experimental sample results can be different from the analytical results due to errors in installing the sample and measurement devices. Nevertheless, the results are consistent. A significant reason for the model's validity is the deformation mode and its agreement with the experimental model, as shown in Fig. 7.

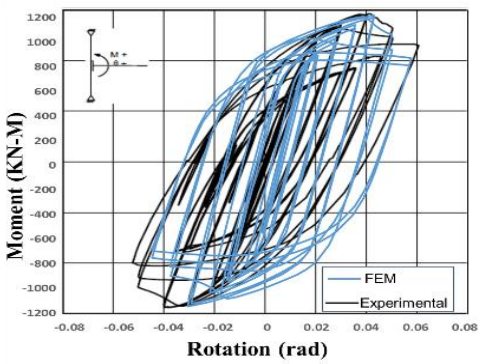


**Fig. 6** Comparison hysteretic curves of experimental & FEM of Sumner specimen [20]

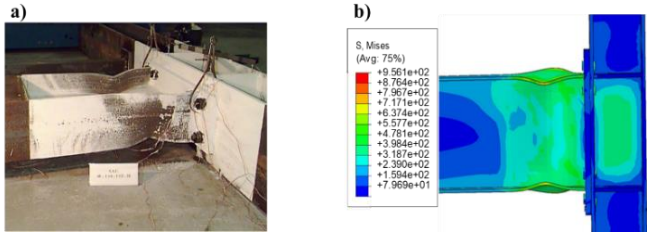


**Fig. 7** Failure mode of the Sumner specimen: (a) experimental [20] & (b) FEM

## 4. FEM evaluation of the two proposed models

### *4.1. Parametric characteristics*

A parametric analysis was carried out to examine the effect of changes in dimensions on the behavior of the two proposed connections. This study was performed in part 3 based on the calibration of the FEM. The IPE270 and IPE360 beam and column were selected for examining the two proposed connections, respectively. The configuration of the bolts consisted of four bolts on the sides of each beam flange. The column height, beam length from its tip to the column center, and bolt diameter was 3 m, 2.5 m, and 20 mm, respectively.

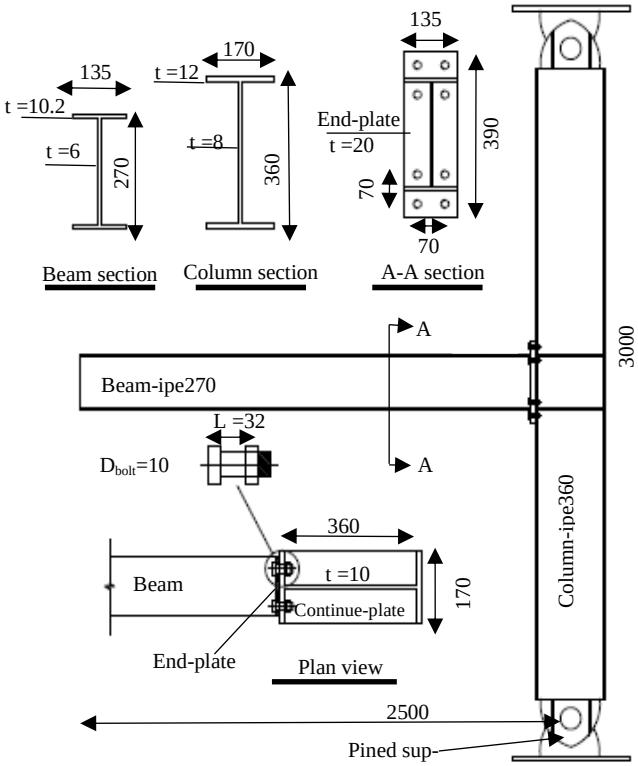


**Fig. 8** End-plate connection details (unit: mm)

Since the two proposed connections are based on the properties of an extended end-plate connection with four bolts on the sides of the beam flange, we examine an end-plate connection with a thickness of 20 mm and a width equal to that of the beam, firstly (Fig. 8). This is carried out to provide a basis for comparison with the two proposed connections. Consequently, the proposed model (I) connection was examined by replacing the end-plate with a pre-built stub section (Fig. 9). Furthermore, the proposed model (II) was examined by combining the pre-built stub with the end-plate (Fig. 10). The minimum and maximum widths of the stub and end-plate are determined according to the widths of the beam flange (135 mm) and the column flange (170 mm). Therefore, IPE270, IPE360, IPB140, and IPB160 sections were used for the stub. Since the IPE's flange width is half its web height, and the IPB section has an equivalent flange width and web height, a difference was observed in behavior. A pre-built stub section with two different numbers was used to examine the effect of web height, flange width, and other section properties. The web and flange were reinforced using stiffeners to compensate for the lack of moment of inertia of the stub section concerning the beam. Three stiffener thicknesses of 10 mm, 12 mm, and 14 mm were considered for each stub. The geometric properties of the analytical samples are presented in Table 3. The sections were designed according to previous research. Moreover, the necessary controls, such as seismic compression of the beam and column sections and the Strong-Column-Weak-Beam (SCWB) rule, were applied. The stub height and bolt configuration were considered unchangeable for all samples, and the bolts were 10.9 degrees M26, based on the high-strength bolts. The modulus of elasticity and Poisson's ratio were 2.05×10e5 MPa and 0.3, respectively. The mechanical properties of the bolts are as follows: $Fy = 994\,MPa$ and $Fu = 1202\,MPa$. Furthermore, the material of other elements such as beam, column, stub, end-plate, and stiffeners was the ST37 steel with a yield strength of $Fy = 240\,MPa$ and the ultimate strength of $Fu = 370\,MPa$.

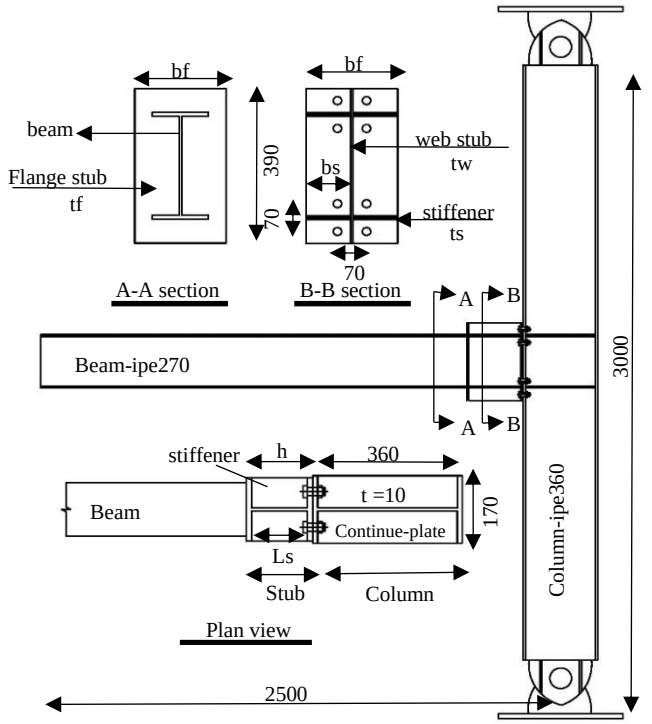


**Fig. 9** Typical details of proposed connection model(I): (unit: mm)

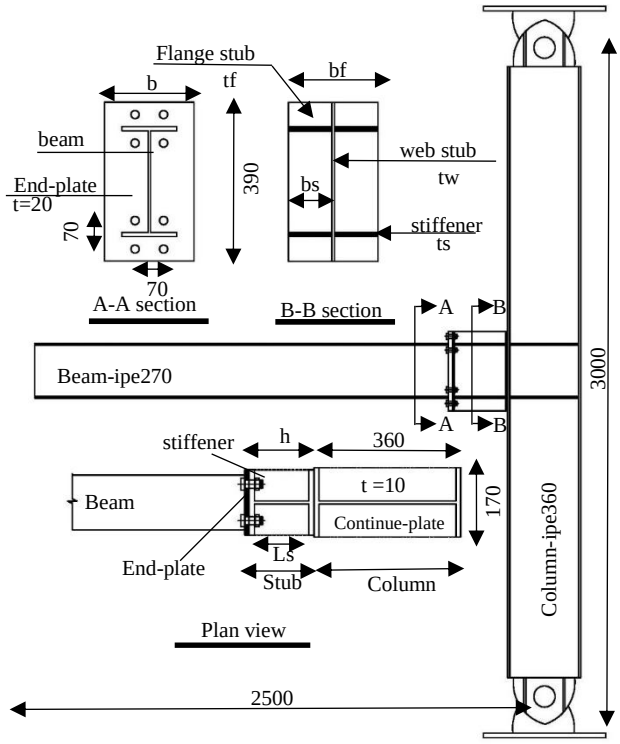


**Fig. 10** Typical details of proposed connection model(II): (unit: mm)

*4.2. Evaluation of results*

The moment-rotation curves of all the samples have been plotted after they were exposed to cyclic loading. The backbone curve was drawn for the moment-rotation curve's positive region, and the bilinear curve was fitted according to FEMA-440 criteria [24].

**Table 3**
Characteristics geometric of the models

| | | Specimen | Stub | | | | Stiffener | | | End-plate | |
|---|---|---|---|---|---|---|---|---|---|---|---|
| | | | h | bf | tf | tw | bs | Ls | ts | t | b |
| Base model | | end-plate | - | - | - | - | - | - | - | 20 | 135 |
| Model I | Set1 | m1-e27-10 | 270 | 135 | 10.2 | 6 | 64.5 | 249.6 | 10 | - | - |
| | | m1-e27-12 | 270 | 135 | 10.2 | 6 | 64.5 | 249.6 | 12 | - | - |
| | | m1-e27-14 | 270 | 135 | 10.2 | 6 | 64.5 | 249.6 | 14 | - | - |
| | | m1-e36-10 | 360 | 170 | 12 | 8 | 81 | 336 | 10 | - | - |
| | | m1-e36-12 | 360 | 170 | 12 | 8 | 81 | 336 | 12 | - | - |
| | | m1-e36-14 | 360 | 170 | 12 | 8 | 81 | 336 | 14 | - | - |
| | Set2 | m1-b14-10 | 140 | 140 | 12 | 7 | 66.5 | 116 | 10 | - | - |
| | | m1-b14-12 | 140 | 140 | 12 | 7 | 66.5 | 116 | 12 | - | - |
| | | m1-b14-14 | 140 | 140 | 12 | 7 | 66.5 | 116 | 14 | - | - |
| | | m1-b16-10 | 160 | 160 | 13 | 8 | 76 | 134 | 10 | - | - |
| | | m1-b16-12 | 160 | 160 | 13 | 8 | 76 | 134 | 12 | - | - |
| | | m1-b16-14 | 160 | 160 | 13 | 8 | 76 | 134 | 14 | - | - |
| Model II | Set1 | m2-e27-10 | 270 | 135 | 10.2 | 6 | 64.5 | 249.6 | 10 | 20 | 135 |
| | | m2-e27-12 | 270 | 135 | 10.2 | 6 | 64.5 | 249.6 | 12 | 20 | 135 |
| | | m2-e27-14 | 270 | 135 | 10.2 | 6 | 64.5 | 249.6 | 14 | 20 | 135 |
| | | m2-e36-10 | 360 | 170 | 12 | 8 | 81 | 336 | 10 | 20 | 170 |
| | | m2-e36-12 | 360 | 170 | 12 | 8 | 81 | 336 | 12 | 20 | 170 |
| | | m2-e36-14 | 360 | 170 | 12 | 8 | 81 | 336 | 14 | 20 | 170 |
| | Set2 | m2-b14-10 | 140 | 140 | 12 | 7 | 66.5 | 116 | 10 | 20 | 140 |
| | | m2-b14-12 | 140 | 140 | 12 | 7 | 66.5 | 116 | 12 | 20 | 140 |
| | | m2-b14-14 | 140 | 140 | 12 | 7 | 66.5 | 116 | 14 | 20 | 140 |
| | | m2-b16-10 | 160 | 160 | 13 | 8 | 76 | 134 | 10 | 20 | 160 |
| | | m2-b16-12 | 160 | 160 | 13 | 8 | 76 | 134 | 12 | 20 | 160 |
| | | m2-b16-14 | 160 | 160 | 13 | 8 | 76 | 134 | 14 | 20 | 160 |

Moreover, yield moment ($M_y$), maximum moment ($M_{max}$), yield drift ($\theta_y$), and maximum drift ($\theta_{max}$, corresponding to $M_{max}$) were obtained. Due to the stability of the two proposed connections system after the drop of the moment-rotation curve, the descending part of the backbone curve up to the 0.8 $M_{pbeam}$ drop was considered the ultimate drift ($\theta_u$) in the parameter calculations for plotting the bilinear curve. Moreover, the maximum and ultimate ductility ($\mu_{max}$, $\mu_u$) are obtained as follows:

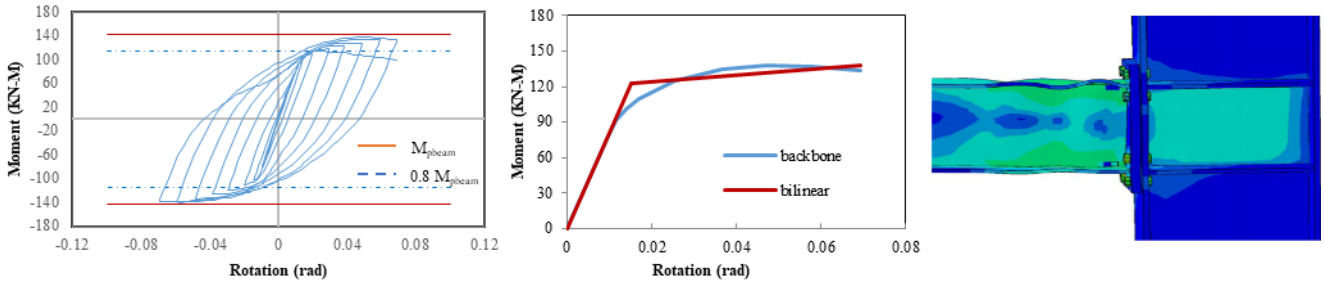


**Fig. 11** Results of End-Plate Connection

$$\mu_{max} = \frac{\theta_{max}}{\theta_y} \quad (1)$$

$$\mu_u = \frac{\theta_u}{\theta_y} \quad (2)$$

Under the requirements of AISC 341-10 [25], in special earthquake resistance systems, the joints must be able to accept a thrust angle of at least 0.04 rad. In this story drift angle, the measured moment of the connection should be equivalent to at least 0.8$M_P$ of the connected beam. $M_P$ is the possible plastic hinge moment.

*4.2.1. End-plate*

The end-plate connection is used as the base model to compare the two proposed connections. According to the analyses, this sample behaves similarly to the connection in part 3. The plastic hinge in the beam is formed at an approximate distance of $d_{beam}/2$ (half of the beam web height) from the column [20]. The moment-rotation, bilinear, and backbone curves and fracture modes are displayed in Fig. 11. At a 4 percent drift, the sample's moment strength is greater than 80% of the plastic moment capacity of the beam. ($M_{0.04}/0.8M_{Pbeam}$=1.2). Moreover, the maximum bending moment strength of the sample is less than the beam's plastic moment capacity ($M_{max}$ / $M_{Pbeam}$ =0.96). Therefore, this connection is classified as rigid, according to AISC 341-10 [19].

*4.2.2. General analysis and discussion of two proposed connections*

A panel zone similar to the column's panel is formed in the stub web in the two proposed connections. Compared to the end-plate connection, it improved ductility and reduced stress in the panel zone of the column. Moreover, the bolted connection of the stub flange with the column, the bolt pry action, creates a plastic hinge between the two rows of bolts. However, this force is considerably lower than the one in the end-plate connection because the front stiffener shares the applied force among all the connection parts by redistributing the strain between the stub flange and the web. The parts extend beyond the beam's height in the connection, act as a stiffener, and transfer considerable moment to the outer bolts. The stub web presence causes more stress transfer over a larger surface of the stub flange bolted to the column flange. Subsequently, a larger area of the column is subjected to compressive stress. Therefore, the stress in the column panel zone decreases. In general, the two proposed connections resist a more significant moment and rotation compared to the end-plate. With an increase in the stiffener's thickness, the maximum moment, ultimate shear, elastic moment, and hardening will increase due to preventing the extended parts of the stub from buckling and the tensile force of the beam flange from resistance. The use of stiffeners in the stub makes it possible for the behavior to mode from semi-rigid to rigid. It is determinable that the connection behavior by changing the thickness of the stiffeners. Two sets of analyses were performed on both proposed model (I) and model (II) connections. Pre-built IPE and IPB sections were used for the first and second sets, respectively. The moment-rotation, bilinear, and backbone curves are shown in Figs. 12 to 19 and the results are summarized in Table 4. The following are observed in the results. The first set (pre-built IPE section), using a stiffener by thickness equivalent to 10mm (ST10), results in the two proposed connections having a fuse-like behavior. As a result, with simultaneous buckling of the stiffeners and the extended part, the stub fails in the compressive region. However, an Increased stiffener thickness (ST12) causes simultaneous buckling in the beam flange and stiffeners, resulting in increased ductility. Finally, by increasing the displacement, a plastic hinge is established in the approximate distance of $d_{beam/2}$ from the stub flange. This means that the plastic hinge in the two proposed connections is further away from the column by a distance equal to the stub's height compared to the end-plate connection. A stiffener with more thickness (ST14) leads to the connection exhibiting a fully rigid behavior and the plastic hinge being created completely within the beam. In comparison between IPE270 and IPE360 sections, used as the stub, the IPE270 section has greater ductility, but the IPE360 section has more bending moment strength. Compared to the end-plate connection, the two proposed connections with an IPE pre-built section have 32% more ductility and 9% more bending strength on average. In the second set (pre-built IPB section), the use of a stiffener by thickness equivalent to 10mm (ST10) has caused a semi-rigid behavior, and the fracture occurs with the simultaneous buckling of the beam flange and stiffener. The two proposed connections exhibit rigid behavior as the stiffener thickness (ST12, ST14) is increased. The behavioral parameters of the IPB140 and IPB160 sections (Table 4) are close. The behavior of the two proposed connections in the second set is unaffected by changes in section and stiffener thickness. Compared to the end-plate connection, the two proposed connections with IPB pre-built section show 13% more ductility and 8% more bending moment strength on average. Comparing the two sets, the IPE section increases the distance of the hinge formed in the beam from the column and increases the resistance against the bending moment due to its larger depth. Moreover, it provides larger deformation compared to IPB due to the thicker stiffeners. The hysteresis loops of all the samples are stable, and that show ductility and energy dissipation are acceptable. In general, the ratios $M_{max}$ / $M_P$ and $M_{0.04}/0.8$ $M_P$ is larger than 1 in all samples except for m1-e27-10 and m2-e27-10. This means that the two proposed connections could transfer all the bending moment of the beam. Furthermore, they exhibit good flexibility and rotational capacities, which satisfies the deformation requirements for rare earthquakes. Therefore, the stub satisfies the criteria for a rigid connection, According to AISC. All the samples are accepted for special moment-resisting frames. The sample fracture modes are displayed in Fig. 20. As evident, in samples where the IPE270 section has been used as the stub, the plastic hinge forms at the stub location, indicating the stub's fuse-like behavior. In other samples, using a stiffener with a thickness of 10 mm leads to the creation of a plastic hinge in the beam. Despite a plastic hinge in the stub in these samples, the connection does not entirely fail and remains stable. Therefore, increasing the stiffener thickness leads to creating the plastic hinge in the beam at approximately $d_{beam}$ /2 from the stub flange. This considerably reduces stress in the connection location, prevents the transient brittle fracture of the weld. It also significantly increases the seismic behavior of the connection. In general, the plastic hinge is formed at a greater distance from the column than the typical end-plate connection. This reduces the stress at the connection location and prevents the transient fracture of the weld, considerably improving the seismic performance of the connection.

*4.2.3. Model (I)*

The following occurs with an increase in the thickness of the stiffeners in the model (I)-set1: The elastic drift ($\theta_y$), elastic bending moment ($M_y$), and maximum bending moment ($M_{max}$) increase, while the maximum drift ($\theta_{max}$) increases with the use of the pre-built IPE270 section as the stub and decreases with the use of the IPE360 section. This indicates the negative effect of the increase in the stub depth on the Model (I) ductility. Furthermore, the maximum ductility $\mu_{max}$ and ultimate ductility $\mu_u$ decrease (considering the descending part of the moment-rotation curve). This decrease is greater when the IPE360 section is used as the stub.

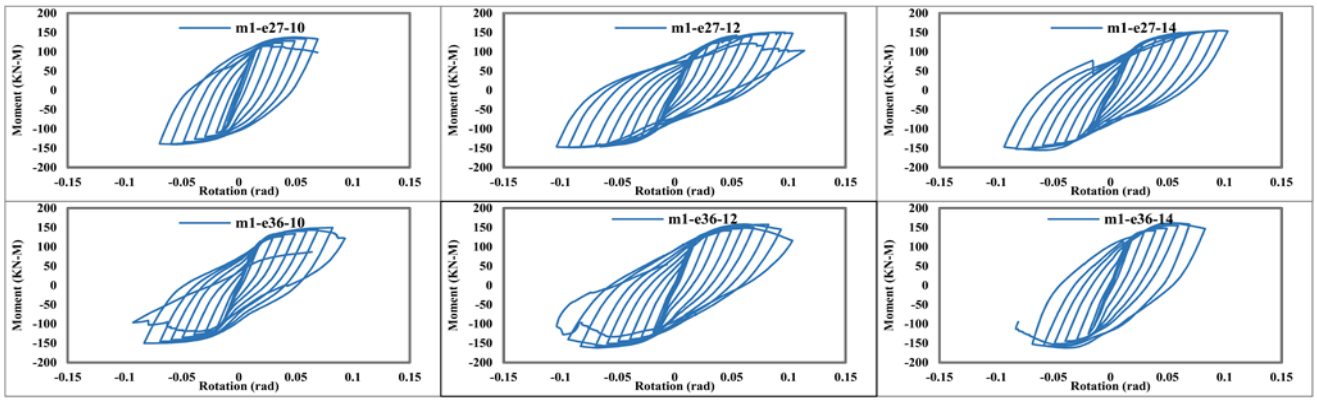


**Fig. 12** Hysteretic curves of model(I)-set1 (IPE sections for stub)

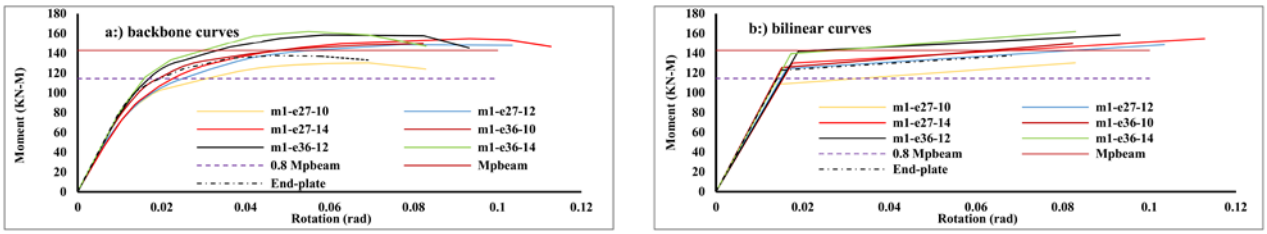


**Fig. 13** Backbone & bilinear of model(I)-set1 (IPE sections for stub)

The largest values of $\mu_{max}$ and $\mu_u$ occur for samples m1-e36-10 and m1-e27-10 with 74% and 47% increases, respectively, compared to the pre-confirmed end-plate connection. The lowest values of these parameters correspond to sample m1-e36-12 with an approximate value equal to the end-plate connection. For all samples except m1-e27-10, $M_{max}$ and My are higher than those in the end-plate connection. The largest values of $M_{max}$ and $M_y$ occur for m1-e36-14 and m1-e36-12 samples with $162\ kN.m$ and $142\ kN.m$, respectively. In model(I)-set2, all the parameters under study exhibit improvement compared to the end-plate connection with small variation ranges. In this set, the largest value of $\theta_{max}$ occurs in m1-b14-10 with a 7.4% drift, and its smallest value occurs in m1-b16-14 with a 4.8% drift. The largest values of $M_{max}$ and $M_y$ occur for m1-b14-12 and m1-b16-14 samples with $153\ kN.m$ and $131\ kN.m$, respectively.

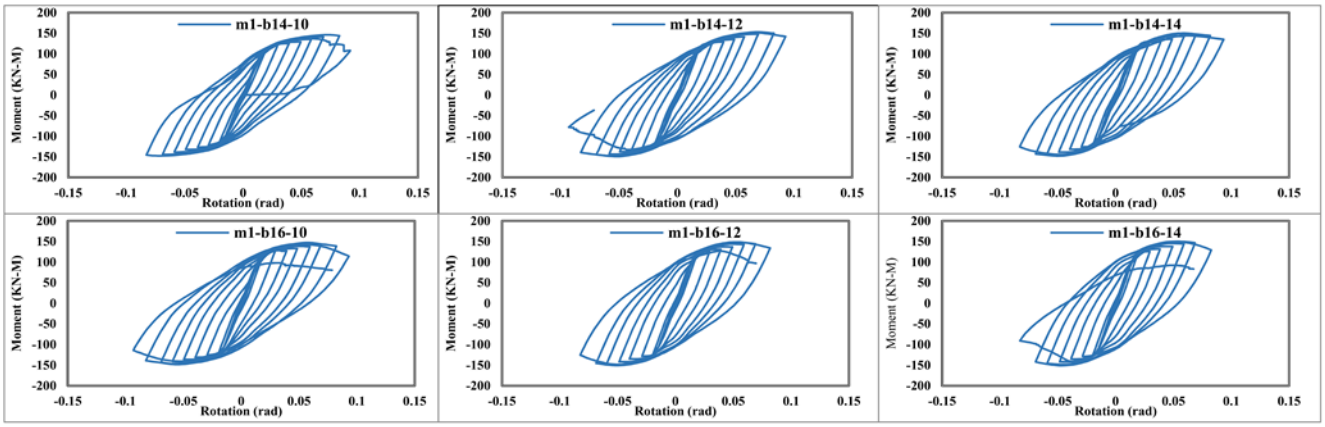


**Fig. 14** Hysteretic curves of model(I)-set2 (for IPB sections for stub)

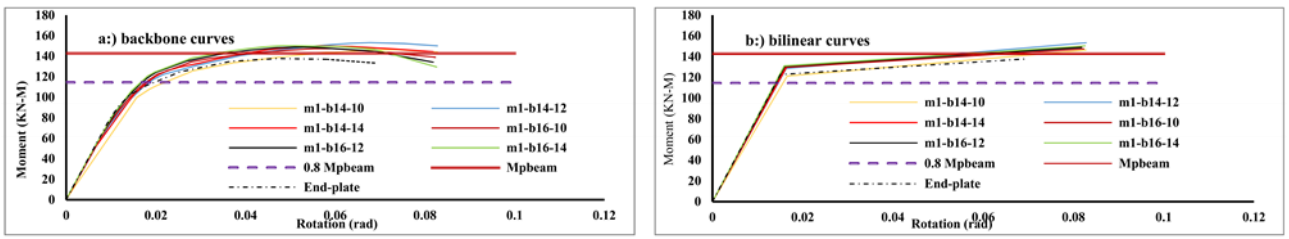


**Fig. 15** Backbone & bilinear of model(I)-set2 (IPB sections for stub)

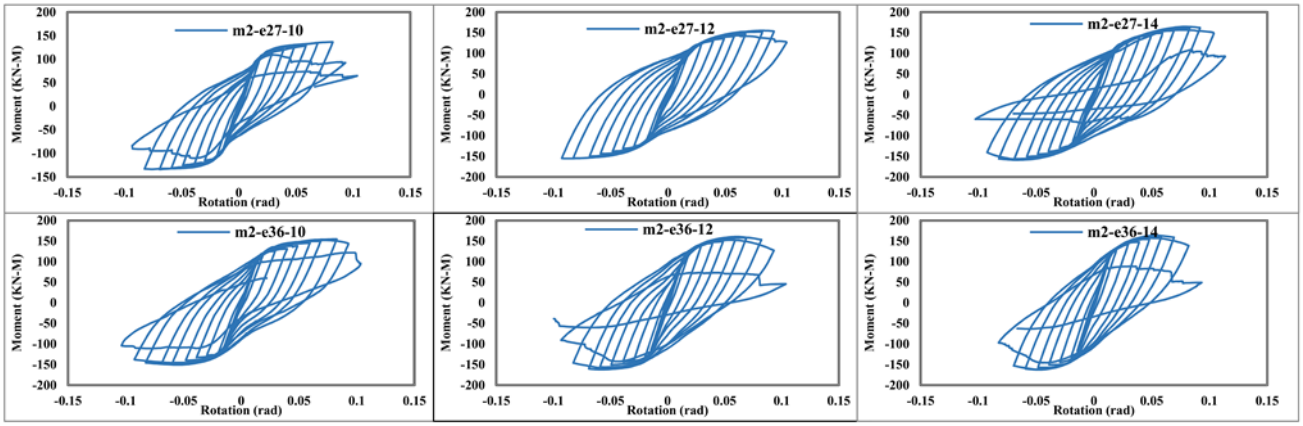


**Fig. 16** Hysteretic curves of model(II)-set1 (IPE sections for stub)

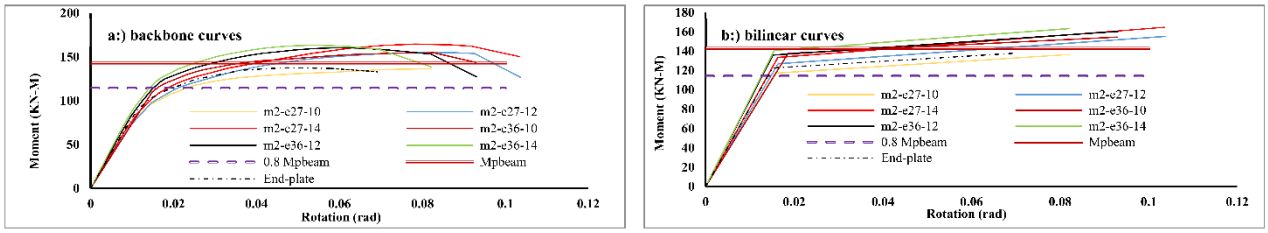


**Fig. 17** Backbone & bilinear of model(II)-set1 (IPE sections for stub)

*4.2.4. Model (II)*

In Model (II)-set1, with an increase in the stiffeners' thickness and the stub depth, the ductility is reduced, and its bending moment strength is increased. In comparison to the end-plate connection, the largest values of $\mu_{max}$ and $\mu_u$ occur for m2-e27-10, and m2-e27-14 samples with 67% and 38% increases, respectively, and these lowest values for these parameters occur for m2-e36-14 and m2-e36-10, with a 10% decrease. The values of $M_{max}$ and $M_y$ are more extensive than those in the end-plate connection for all samples in this set except for m2-e27-10. The largest values of $M_{max}$ and $M_y$ occur for sample m2-e36-14 with the values of $163\ kN.m$ and $141\ kN.m$. The samples in Model(II)-set2 generally have a smaller ductility compared to other samples. In this set, an increase in the stiffener thickness and stub depth led to increased ductility, unlike in other samples. The largest values of $M_{max}$ and $M_y$ corresponding to sample m2-b16-14 are $155\ kN.m$ and $139\ kN.m$, respectively. The noteworthy point in Model(II)-set2 is the relative increase in the elastic drift ($\theta_y$) compared to other samples. The most considerable value of this parameter belongs to sample m2-b14-10, which has a 2.2% drift and is 48% more than the value in the end-plate connection.

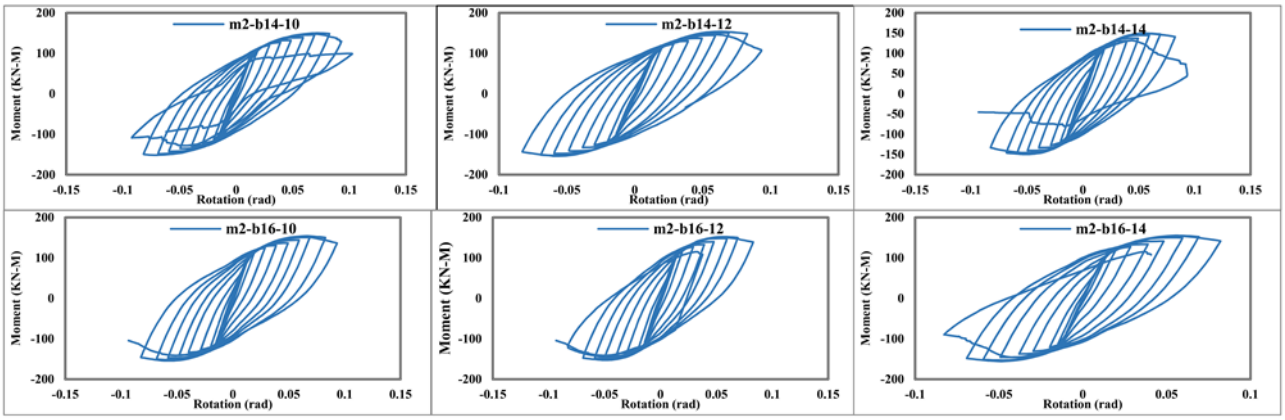


**Fig. 18** Hysteretic curves of model(II)-set2 (IPB sections for stub)

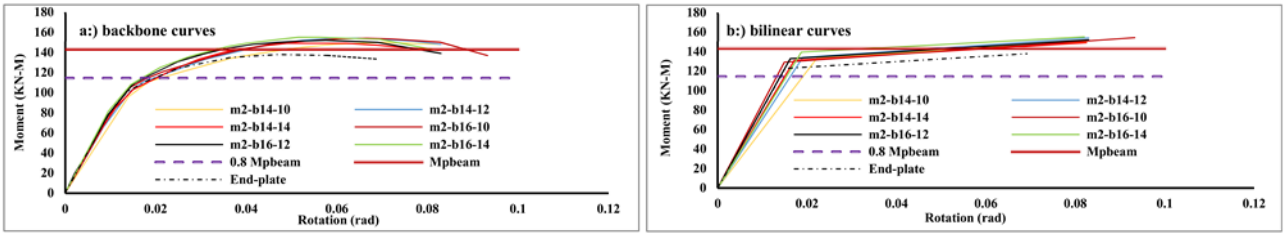


**Fig. 19** Backbone & bilinear of model(II)-set2 (IPB sections for stub)

*4.3. Evaluation of equivalent plastic strain (PEEQ)*

The primary purpose of the two proposed connections is to reduce non-elastic deformations in the column. The non-elastic rotation in massive earthquakes causes local buckling and excessive lateral torsional buckling in the panel zone.

This potential fracture mode must be considered besides the bending buckling of the columns. Therefore, the performance of the connections under seismic loading is somewhat dependent on the panel zone behavior. Moreover, reducing the plastic strain in this area prevents the fracture of the panel zone and improves the connection's behavior. The equivalent plastic stress (PEEQ) index is used to compare the effect of the two proposed connections on the panel zone. This index is used as a tool for measuring the ductility at the local surface. It is calculated as follows:

$$PEEQ=\frac{\sqrt{\frac{2}{3}\varepsilon_{ij}^{p}\varepsilon_{ij}^{p}}}{\varepsilon_{y}} \quad (3)$$

Where $\varepsilon_{ij}^{p}$ is the component of plastic strain in the direction specified by i and j and $\varepsilon_y$ is yield strain under uniaxial monotonic tensile loading, respectively. In this study, the panel zone is the surface between the two continuity plates in the column web. To evaluate the PEEQ index, the curve of its maximum value was plotted and compared for the points on the panel zone surface. These curves are shown in Figs. 21 & 22. According to these curves, the equivalent plastic strain PEEQ in the end-plate connection is zero up to a drift of 1.5 percent (cycle=15), indicating the absence of yielding in the column panel zone. However, after this point, the value of PEEQ increases. In model(I)-set1, the use of the IPE270 section as the stub reduces the PEEQ in the panel zone to a great extent. A stiffener with a thickness of 10 mm decreases the PEEQ by 80% at a 6% drift (cycle=20). This is due to the fuse-like performance of the stub in this sample. With an increase in the stiffener's thickness to 12 mm and 14 mm, the value of PEEQ dropped by 60% and 40%, respectively. The IPE360 section's use as the stub with a 10 mm stiffener results in a 40% reduction in PEEQ. In this sample (m1-e36-10), the plastic hinge is formed in the stub. However, an increase in the stiffener thickness to 12 mm and 14 mm increased the connection's rigidity and increased PEEQ compared to the end-plate connection. In model(I)-set2, the IPB section's use reduced the PEEQ index by 40%. IPB140 and IPB160 sections as the stub with 10 mm, 12 mm, and 14 mm stiffeners do not significantly affect this index. This shows that the stub behaves more stably and reliably with the IPB section. Model (II) will considerably reduce PEEQ in the panel zone. This reduction occurred for all samples. In Model (II)-set1, the largest and smallest PEEQ values belonged to m2-e36-st14 and m2-e27-10 with 20% and 95% reductions, respectively, at a 6% drift. The reduction in PEEQ is continued in model (II)-set2 using the IPB section as the stub. The analytical samples with this section showed similar behaviors, and the PEEQ index decreased by approximately 80% at a 6% drift compared to the end-plate connection. Comparing the two proposed models shows that PEEQ is lower by 30% in model (II) than model (I). The second mode is when both the beam and the stub enter the plastic phase.

## 5. Design method

The parameters affecting the SSC connection's behavior allow the designer to design the connection according to the performance requirements of the structure. The SSC connection is capable of acting as a fuse. Therefore, the most important point in its design is determining the required bending moment. Three modes are considered for the behavior of the SSC connection. The first mode is when the SSC connection behaves as fully rigid, and the plastic hinge is formed in the beam. In this mode, the design bending moment is equal to the plastic bending moment of the beam at the plastic hinge (using the 14mm stiffener).

**Table 4**
Summary of numerical test results.

| Specimen | | | $\theta_y$ | $\theta_{max}$ | $\theta_u$ | $M_y$ | $M_{max}$ | $M_{0.04rad}$ | $\mu_{max}$ | $\mu_u$ | $M_{max}/M_{Pbeam}$ | $M_{0.04}/0.8\ M_{Pbeam}$ |
|---|---|---|---|---|---|---|---|---|---|---|---|---|
| | | | rad | | | kN.m | | | | | | |
| Base model | | end-plate | 0.015 | 0.047 | 0.069 | 123 | 138 | 137 | 3.12 | 4.58 | 0.96 | 1.2 |
| model I | set1 | m1-e27-10 | 0.013 | 0.069 | 0.09 | 108 | 130 | 124 | 5.17 | 6.72 | 0.91 | 1.18 |
| | | m1-e27-12 | 0.016 | 0.077 | 0.103 | 124 | 149 | 135 | 4.73 | 6.37 | 1.04 | 1.26 |
| | | m1-e27-14 | 0.018 | 0.093 | 0.09 | 130 | 155 | 138 | 5.29 | 5.1 | 1.08 | 1.27 |
| | | m1-e36-10 | 0.015 | 0.082 | 0.09 | 125 | 150 | 139 | 5.43 | 5.93 | 1.05 | 1.24 |
| | | m1-e36-12 | 0.019 | 0.059 | 0.093 | 142 | 158 | 150 | 3.1 | 4.92 | 1.11 | 1.27 |
| | | m1-e36-14 | 0.017 | 0.055 | 0.09 | 139 | 162 | 155 | 3.19 | 5.22 | 1.13 | 1.28 |
| | set2 | m1-b14-10 | 0.017 | 0.074 | 0.083 | 121 | 146 | 135 | 4.47 | 5 | 1.02 | 1.08 |
| | | m1-b14-12 | 0.016 | 0.068 | 0.083 | 129 | 153 | 144 | 4.14 | 5.06 | 1.07 | 1.18 |
| | | m1-b14-14 | 0.016 | 0.056 | 0.082 | 130 | 150 | 145 | 3.43 | 4.98 | 1.05 | 1.21 |
| | | m1-b16-10 | 0.016 | 0.059 | 0.082 | 130 | 147 | 142 | 3.69 | 5.12 | 1.03 | 1.22 |
| | | m1-b16-12 | 0.016 | 0.051 | 0.082 | 131 | 149 | 145 | 3.16 | 5.1 | 1.04 | 1.31 |
| | | m1-b16-14 | 0.016 | 0.048 | 0.083 | 131 | 150 | 147 | 3.05 | 5.2 | 1.05 | 1.35 |
| model II | set1 | m2-e27-10 | 0.016 | 0.082 | 0.082 | 117 | 137 | 128 | 5.22 | 5.22 | 0.96 | 1.12 |
| | | m2-e27-12 | 0.016 | 0.082 | 0.104 | 127 | 155 | 139 | 4.99 | 6.34 | 1.09 | 1.22 |
| | | m2-e27-14 | 0.016 | 0.078 | 0.104 | 134 | 165 | 146 | 4.8 | 6.36 | 1.15 | 1.28 |
| | | m2-e36-10 | 0.019 | 0.072 | 0.093 | 138 | 155 | 145 | 3.87 | 5 | 1.08 | 1.27 |
| | | m2-e36-12 | 0.015 | 0.059 | 0.093 | 136 | 161 | 154 | 3.89 | 6.13 | 1.12 | 1.35 |
| | | m2-e36-14 | 0.015 | 0.053 | 0.082 | 141 | 163 | 159 | 3.41 | 5.31 | 1.14 | 1.39 |
| | set2 | m2-b14-10 | 0.022 | 0.07 | 0.083 | 134 | 150 | 137 | 3.14 | 3.7 | 1.05 | 1.2 |
| | | m2-b14-12 | 0.019 | 0.06 | 0.083 | 134 | 154 | 143 | 3.12 | 4.36 | 1.08 | 1.25 |
| | | m2-b14-14 | 0.017 | 0.054 | 0.083 | 131 | 149 | 145 | 3.15 | 4.81 | 1.04 | 1.27 |
| | | m2-b16-10 | 0.015 | 0.067 | 0.093 | 129 | 154 | 146 | 4.46 | 6.25 | 1.08 | 1.28 |
| | | m2-b16-12 | 0.016 | 0.058 | 0.083 | 133 | 152 | 147 | 3.54 | 5.11 | 1.06 | 1.28 |
| | | m2-b16-14 | 0.019 | 0.062 | 0.082 | 139 | 155 | 149 | 3.31 | 4.38 | 1.08 | 1.3 |

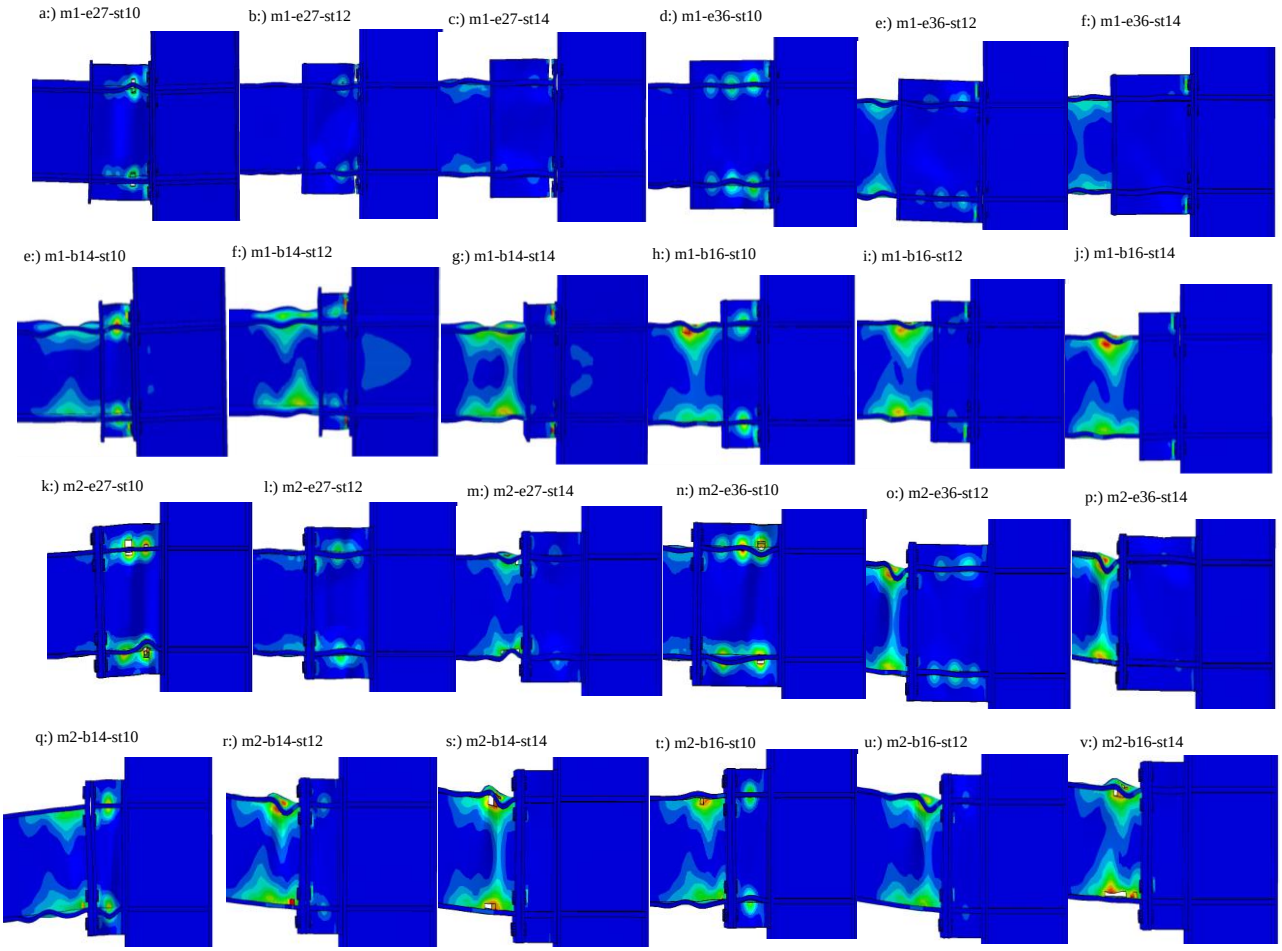


**Fig. 20** Equivalent Plastic Strain (PEEQ) of Stub Models

The second mode is when both the beam and the stub enter the plastic phase. In this mode, the two proposed connections have the highest ductility (the use of the 12mm stiffener), and the design bending moment is at most equivalent to the plastic bending moment of the beam ($M_{pbeam}$). The third mode is when the plastic hinge is formed in the stub, and the connection acts as a fuse. In this mode, the design bending moment is between 0.8 $M_{pbeam}$ and $M_{pbeam}$. According to the results of this investigation, the stub depth and stiffener thickness are the main parameters determining the behavior of the two proposed connections. The stub web behaves like the column panel zone, and the stiffeners behave similarly to the continuity plates. Thus, they can be designed based on the column panel zone rules. The other connection components, such as stiffeners, bolts, and end-plates, are designed according to the requirements of reputable rules. However, given the complexity of the exact design equations, in this study, some engineering rules are suggested for SSC connections as follows:

- In general, all the sections must be controlled concerning the width-to-thickness b/t regulations for compressed elements in highly ductile members, according to ANST/AISC341-16.
- The web and flange stub thicknesses are recommended to be at least equivalent to those of the beam.
- The stub flange width must be at least equal to the width of the beam flange and at most equivalent to the width of the column flange.
- The stub section's depth is recommended to be at least half the beam height
- and equal to the beam height. This value must not be less than 120 mm due to practical considerations.
- The stub height is recommended to be equal to the sum of the beam depth and $6d_{bolt}$ to 8 $d_{bolt}$.
- The bolt arrangement is controlled by the end-plate design rules as well as practical considerations. The distances of the bolt hole centers from the stub web and beam flange surfaces are recommended to be at least two times and, at most, three times the bolt diameter.

## 6. Conclusions

In this research, using Rolled profiles, two novel steel connections with new construction that aims to reduce damage to beams and columns and reduce plastic strain in the panel zone have been proposed. With a load transfer mechanism different from those of conventional connections, the proposed construction consists of a stub that is placed as a short column between the column and the beam (or welded beam to the end-plate) and was named Short Stub Column (SSC). The first proposed model could be an alternative to the end-plate connection, and the second proposed model could be an alternative to the tree connection.

For parametric evaluation, two sets of analyzes were performed with Pre-built IPE, and IPB sections were used for both proposed connections. The FEM software was employed to simulate 24 submodules in two sets. After each sample was subjected to cyclic loading, the moment-rotation curves were plotted, and the backbone & bilinear curves were drawn.

Based on the results obtained, the $M_{0.04}$ / 0.8 $M_{Pbeam}$ ratio is more than one for all samples. Therefore, they provide AISC requirements for use in special moment frames. Also, by changing the stiffeners' thickness, it can be determined whether the plastic hinge is formed in the beam or the stub.

The reduction in strength of the samples is due to the fracture and local ductile buckling during cyclic loading, and no global fracture is observed in the samples.

FEM studies on the SSC connection indicate that this connection has excellent ductility. The stub region absorbs considerably more energy than the hinge in the beam due to its plastic performance. It creates a limited and controlled hinge with excellent ductility, increasing the structure's period and behavior factor. Compared to conventional bending moment connections, not only does this connection not show reduced ultimate strength and hardening, but its plastic rotation capacity can also be increased several times. Timely yielding in the stub causes a fuse-like behavior. It prevents damage to the beam and column, significantly reducing the plastic stress and strain in the panel zone and improving energy dissipation reliability. Also, this investigation of the peeq index in the panel zone showed that the SSC connection reduces the plastic strain compared to the end-plate connection.

## Acknowledgments

This research has conducted in collaboration with the National Iranian South Oil Company.

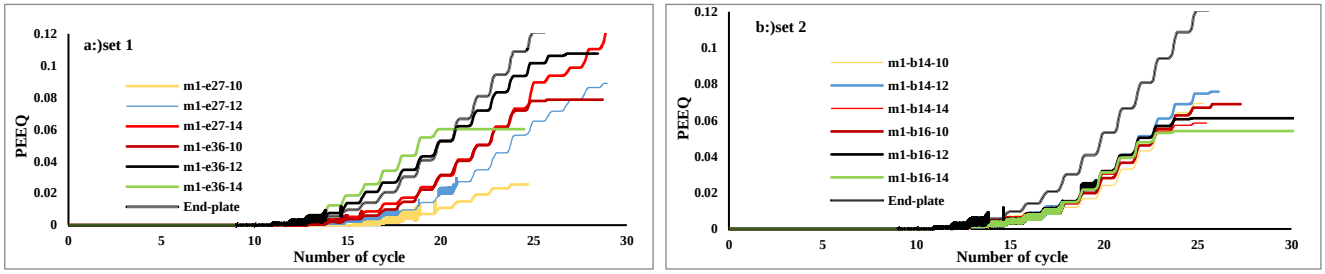


**Fig. 21** PEEQ curves of model(I)

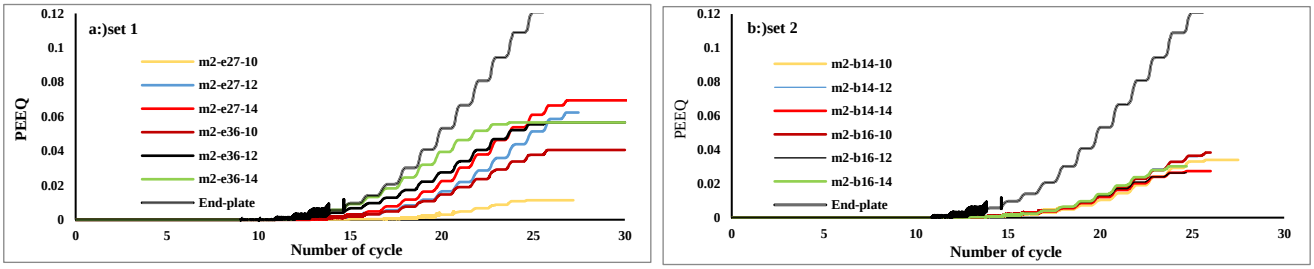


**Fig. 22** PEEQ curves of model(II)

## References


[1] Moghadam A, E Estekanchi H, Yekrangnia M. Evaluation of PR steel frame connection with torsional plate and its optimal placement. Scientia Iranica. 2018 Jun 1;25(3):1025-38.

[2] SAC J. State of the art report on connection performance Report No FEMA-355D. Federal Emergency Management Agency (FEMA), Washington. 2000.

[3] Alhendi H, Celikag M. Finite element prediction of reverse channel connections to tubular columns behavior. Engineering Structures. 2015 Oct 1;100:599-609.

[4] Mirghaderi SR, Torabian S, Keshavarzi F. I-beam to box–column connection by a vertical plate passing through the column. Engineering Structures. 2010 Aug 1;32(8):2034-48.

[5] Miller DK. Lessons learned from the Northridge earthquake. Engineering structures. 1998 Apr 1;20(4-6):249-60.

[6] Tremblay R, Filiatrault A, Timler P, Bruneau M. Performance of steel structures during the 1994 Northridge earthquake. Canadian Journal of Civil Engineering. 1995 Apr 1;22(2):338-60.

[7] Tremblay R, Filiatrault A, Bruneau M, Nakashima M, Prion HG, DeVall R. Seismic design of steel buildings: lessons from the 1995 Hyogo-ken Nanbu earthquake. Canadian Journal of Civil Engineering. 1996 Jun 1;23(3):727-56.

[8] American Institute of Steel Construction (AISC), Seismic Provisions for Structural Steel Buildings, AISC ANSI/AISC 341-16, Chicago, IL, 2016.

[9] Garoosi AM, TahamouliRoudsari M, Hashemi BH. Experimental evaluation of rigid connection with reduced section and replaceable fuse. InStructures 2018 Nov 1 (Vol. 16, pp. 390-404). Elsevier.

[10] Behrooz SM, Erfani S. Parametric study of Stub-Beam Bolted Extended End-Plate connection to box-columns. Journal of Constructional Steel Research. 2020 Aug 1;171:106155.

[11] Shen Y, Christopoulos C, Mansour N, Tremblay R. Seismic design and performance of steel moment-resisting frames with nonlinear replaceable links. Journal of Structural Engineering. 2011 Oct 1;137(10):1107-17.

[12] Li X. Moment-rotation behaviour of universal beam to tubular column connections using reverse channel. The University of Manchester (United Kingdom); 2012.

[13] O.Yılmaz, S Bekiroğlu. Performance Evaluation of Weak-Axis Steel Moment Connections. XVI INTERNATIONAL SCIENTIFIC CONFERENCE VSU'2016.

[14] Hu G, Huang W, Xie H. Mechanical behavior of a replaceable energy dissipation device for precast concrete beam-column connections. Journal of Constructional Steel Research. 2020 Jan 1;164:105816.

[15] Peng H, Ou J, Mahin S. Design and numerical analysis of a damage-controllable mechanical hinge beam-to-column connection. Soil Dynamics and Earthquake Engineering. 2020 Jun 1;133:106149.

[16] Shi Q, Yan S, Kong L, Bu X, Wang X, Sun H. Seismic behavior of semi-rigid steel joints—Major axis T-stub and minor axis end-plate. Journal of Constructional Steel Research. 2019 Aug 1;159:476-92.

[17] Jiang J, Chen S. Experimental and numerical study of double-through plate connections to CFST column. Journal of Constructional Steel Research. 2019 Feb 1;153:385-94.

[18] Zhang Y, Li Q, Zhuge Y, Liu A, Zhao W. Experimental study on spatial prefabricated self-centering steel frame with beam-column connections containing bolted web friction devices. Engineering Structures. 2019 Sep 15;195:1-21.

[19] Liu Y, Huang SS, Burgess I. Component-based modelling of a novel ductile steel connection. Engineering Structures. 2020 Apr 1;208:110320.

[20] Sumner EA. Unified design of extended end-plate moment connections subject to cyclic loading (Doctoral dissertation, Virginia Tech).

[21] British Standards Institution. Mechanical Properties of Fasteners Made of Carbon Steel and Alloy Steel: Set Screws and Similar Threaded Fasteners Not Under Tensile Stresses. British Standards Institution; 1999.

[22] ASCE/SEI Seismic Rehabilitation Standards Committee. Seismic rehabilitation of existing buildings. ASCE/SEI. 2007:41-06.

[23] Venture SJ. SAC. Protocol for Fabrication, Inspection, Testing and Documentation of Beam-Column Connection Test and Other Experimental Specimens. SAC Rep. SAC/BD-97/02, Sacramento, California; 1997.

[24] FEMA A. 440, Improvement of nonlinear static seismic analysis procedures. FEMA-440, Redwood City. 2005;7(9):11.

[25] AISC A. AISC 341-10. Seismic Provisions for Structural Steel Buildings, American Institute of Steel Construction. Inc., Chicago, IL. 2010.